Improving efficiency of transcritical CO_2 cycles through a magnetic refrigeration subcooling system

Laura Nebot-Andrés*[, a], Manuel Gesù Del Duca[b], Ciro Aprea[b], Andrej Žerovnik[c], Jaka Tušek[c], Rodrigo Llopis [a], Angelo Maiorino[b]

[a] Thermal Engineering Group, Mechanical Engineering and Construction Department, Jaume I University, Spain

[b] Department of Industrial Engineering, Università di Salerno, Via Giovanni Paolo II, 132, 84084 Fisciano, Salerno, Italy

[c] Faculty of Mechanical Engineering, University of Ljubljana, Aškerčeva 6, 1000 Ljubljana, Slovenia

*Corresponding author: lnebot@uji.es, +34 964 718133

Abstract

Subcooling methods for transcritical CO_2 plants are being studied in order to improve the behaviour of these systems in hot climates, where basic configurations are not competitive enough. To achieve important improvements in the transcritical CO_2 performance, it is necessary to perform the subcooling with a refrigeration cycle working with a Coefficient of Performance higher than that of the CO_2 system without subcooling. Magnetic refrigeration devices can achieve high Coefficient of Performance values when the temperature difference between the hot sink and cold source is small, and therefore they meet the requirements to be applied as a CO_2 subcooling method. This work presents the coupling of two refrigeration technologies: vapour compression and magnetocaloric refrigeration, which has not yet been presented in the literature. The magnetic refrigeration system is, based on the experimental results of the existing prototype, analysed semi-empirically and further evaluated, as a subcooling method for a transcritical CO_2 cycle in a wide range of ambient conditions. Gas-cooler pressure, subcooling degree and operating parameters of the magnetic refrigerator were optimized for each condition to obtain the maximum Coefficient of Performance. We show that subcooling with the existing prototype of magnetic refrigeration system can enhance the overall Coefficient of Performance of transcritical CO_2 cycle by up to 9%.

Keywords

Carbon Dioxide, Transcritical, Magnetic refrigeration, Subcooling, Modelling, Optimization

Nomenclature

AMR	active magnetic regenerator
APP	temperature approach, K
BP	back-pressure valve
COP	coefficient of performance
EXV	electronic expansion valve
GWP	global warming potential
h	specific enthalpy, $kJ \cdot kg^{-1}$
$\dot{m}$	mass flow rate, $kg \cdot s^{-1}$
MCM	magnetocaloric material
MR	magnetic refrigeration
MRS	magnetic refrigeration subcooling
p	absolute pressure, bar

Pc	power consumption, kW
$\dot{Q}$	cooling capacity, kW
SUB	degree of subcooling produced in the subcooler, K
T	temperature, ºC

Greek symbols

b	biases of the hidden and output neurons
ρ	density, kg·m^{-3}
τ	blow period, s
η	efficiency
v	specific volume, m^3·kg^{-1}
Δ	increment
Δt	temperature difference
w	synaptic weights

Subscripts

C	cold
CO_2	corresponding to the CO_2 cycle
dis	compressor discharge
env	corresponding to the environment
gc	gas-cooler
ht	heat transfer fluid
H	hot
i	isentropic/ideal/internal
in	inlet
mag	corresponding to the magnetic system
main	corresponding to the main cycle
max	maximum
min	minimum
MR	corresponding to the magnetic refrigerator
0	evaporating level
o	outlet
s	isentropic
span	temperature span
sub	subcooler
suc	suction
v	volumetric

1. Introduction

Nowadays, carbon dioxide is the reference refrigerant used in most of centralized refrigeration applications for commercial purposes. Despite being a natural refrigerant used since the beginning of refrigeration, its use has been boosted in recent years due to regulations that restrict the use of most refrigerants in some applications of refrigeration (European Commission, 2014; UNEP/TEAP, 1999). Carbon dioxide is a refrigerant that meets the limitations because its global warming potential (GWP) equals to 1 and it can be

used in safety conditions since it is neither toxic nor flammable. Despite its great potential, its performance under certain working conditions can be significantly lower compared to fluorinated refrigerants used so far.

In recent years, complex cycles have been developed with the aim of improving its energy performance, especially for areas where the heat rejection temperature is high because the energy behaviour of CO_2 systems drops significantly when the heat rejection temperature is higher than 15 ºC (Hafner A. et al., 2014). The adoption of natural refrigerants such as CO_2 and NH_3 in complex systems for commercial application outperform other systems in extreme warm climates (Purohit et al., 2018). Researchers have been working in different lines of research, as the use of ejectors (Hafner A. et al., 2014; Lawrence and Elbel, 2016; Lawrence and Elbel, 2019), the combination with other systems (Aprea et al., 2015; Arora et al., 2011; Karampour and Sawalha, 2016) and the parallel compression (Sarkar and Agrawal, 2010). Another line of research that has been intensively developed in recent years is CO_2 subcooling (Llopis et al., 2018). Different subcooling methods have been studied and they can be classified in two types: dedicated or integrated subcooling. The aim of the subcooling is to enhance the specific cooling capacity and the Coefficient of Performance (COP) of the refrigeration system. It reduces the optimum gas-cooler pressure, which leads to a reduction of the power consumption of the compressor and an increase of the refrigerant mass flow rate.

Among the integrated systems, the best known is the use of the internal heat exchanger (IHX), which subcools the CO_2 at the exit of the gas-cooler and reheats the vapour before the compressor suction point (Rigola et al., 2010). The integrated mechanical subcooling system performs the subcooling of the CO_2 since a part of the CO_2 flow that is extracted from the main cycle is expanded and then taken to the subcooler, which is placed downstream of the gas-cooler. This flow is then recompressed by an auxiliary compressor and reinjected to the main cycle (Nebot-Andrés et al., 2020a).

The dedicated methods have the same operating principle but subcooling is caused by a backup cycle, external to the main CO_2 cycle. The dedicated mechanical subcooling (Beshr et al., 2016; Bush et al., 2017; Llopis et al., 2016; Nebot-Andrés et al., 2020b) is the most studied one and performs the subcooling using an external vapour compression cycle that is thermally coupled to the main cycle through the subcooler and works with a refrigerant different from CO_2. Since the results obtained theoretically and experimentally for this cycle were very promising, other dedicated systems have been developed. For example, for smaller cooling capacity systems, the use of thermoelectric modules providing the subcooling has been studied (Astrain et al., 2019). Experimentally, increments with regard to the cycle without subcooling of 6.3% at 25°C of ambient temperature and 9.9% at 30°C were obtained for an evaporative temperature of −10 °C (Sánchez et al., 2020).

Similar to the dedicated subcooling systems presented to date, there is a possibility of applying new technologies to the CO_2 cycle to perform the subcooling. Magnetic refrigeration (MR) is an emerging technology that uses a solid as a refrigerant, taking advantage of the magnetocaloric effect (MCE). The MCE is a feature of some magnetic materials, which heat up when they are subjected to an external magnetic field, and cool down after the removal of the applied field. They are called magnetocaloric materials (MCMs). The MCE value can be represented as the isothermal entropy change Δs_{iso} or the adiabatic temperature change ΔT_{ad} of the MCM induced by the augmenting or the diminishing of the external magnetic field which the material is subjected to. If the conditions are kept adiabatic, the temperature of MCM increases by the ΔT_{ad}. On the other hand, if the conditions are kept isothermal, the specific entropy of MCM decreases by the Δs_{iso}.

Magnetic refrigeration devices can achieve higher efficiencies than those of vapour compression systems, as long as they work with a relatively low temperature difference between the heat sink and cold source (Aprea et al., 2016; Dall'Olio et al., 2021; Eriksen et al., 2015; Kamran et al., 2020; Lozano et al., 2016; Masche et al., 2021; Masche et al., 2022). Furthermore, magnetic refrigeration systems are considered as environmental-friendly technologies since they use a solid substance as a refrigerant in substitution of the

ozone depleting and greenhouse effect gases used in vapour compression applications. The use of active magnetic regenerators (AMR), which is nowadays a key element of MR devices, was proposed by Barclay (1982) and it allowed overcoming the limitations regarding the small adiabatic temperature change showed by the most commonly used MCMs. The AMR cycle is based on four operational steps: an adiabatic magnetisation, an isofield cooling, an adiabatic demagnetisation and an isofield heating. During the first step, the MCM in the AMR is subjected to the external magnetic field that increases its temperature due to MCE. Then, keeping the magnetic field at a constant value, a fluid flows through the material absorbing heat from it, which is rejected in the hot heat exchanger. In the adiabatic demagnetisation step, the external magnetic field is removed, and the MCM cools down. At the last step of the cooling cycle, with no external magnetic field, the fluid flows in a counter-flow direction through the material, expelling heat to it. Next, the fluid absorbs heat in the cold heat exchanger. At this point, the steps are repeated. To date around 100 prototype of magnetic refrigeration devices have been developed around the world (Greco et al., 2019).

As presented in Llopis et al. (2018), the CO_2 systems will improve their COP as long as the COP of the auxiliary cycle is higher than the COP of the cycle without subcooling. The dedicated cycle performs heat rejection to the same hot sink as the CO_2 cycle and the cold source is defined by the temperature at the exit of the gas-cooler and the subcooling degree. That means that temperature difference between the hot sink and the cold source of the auxiliary cycle are rather small. Since the MR devices can operate with high COP values at small temperature span, they can be well suited for subcooling of the CO_2 system. In addition, MR uses environmentally friendly materials, and the environmental impact of the system would remain low.

The objective of this work is to evaluate the possibilities of merging these two technologies from a first law general approach and to quantify the improvements that could be obtained. The main objective is to perform the thermodynamic analysis of a CO_2 cycle subcooled by a MR and analyze the behavior of the main energetic parameters of the coupling for different ambient temperatures. Optimum conditions must be found in order to optimize the operation of this cycle, where following parameters that must be controlled are gas-cooler pressure, subcooling degree, mass flow rate and operating frequency of the MR. The results presented in this work correspond to the evaluation of the cycle for a range of environmental temperatures between 25 ºC and 35 ºC, always at the operating conditions that maximize the COP, and for an evaporation temperature of -15 ºC. The overall COP as well as an in-depth study of the operating parameters of the MR system is presented. A comparison with the cycle without subcooling is also shown and the improvements that can be obtained are quantified.

2. Methods

A transcritical CO_2 refrigeration cycle as shown in Figure 1 is considered to evaluate the benefits of performing the CO_2 subcooling by a MR. The CO_2 system performs the expansion process in two stages with a liquid receiver in between both (points 4 to 7). The first expansion device is a back-pressure valve (BP, points 4 to 5) and controls the discharge pressure, while the second expansion valve (EXV, points 6 to 7) controls the evaporating process. The liquid receiver is placed between both valves (points 5 to 6). Subcooling is performed in a subcooler (points 3 to 4) placed after the gas-cooler (2 to 3), which thermally connects the CO_2 cycle and the heat transfer fluid of the MR device.

The magnetic refrigeration system is made of a single-layer Gadolinium AMR with water as heat transfer (regenerative) fluid. It should be noted that magnetocaloric materials act as a refrigerant in the MR technology and water is only used as a heat transfer medium. Other heat transfer medium would in general also be possible, but water is cheap, environmentally friendly and has good heat transfer properties. Both cycles, the CO_2 transcritical and the MR one, perform the heat rejection to the same hot sink, which is considered to be the environmental temperature.

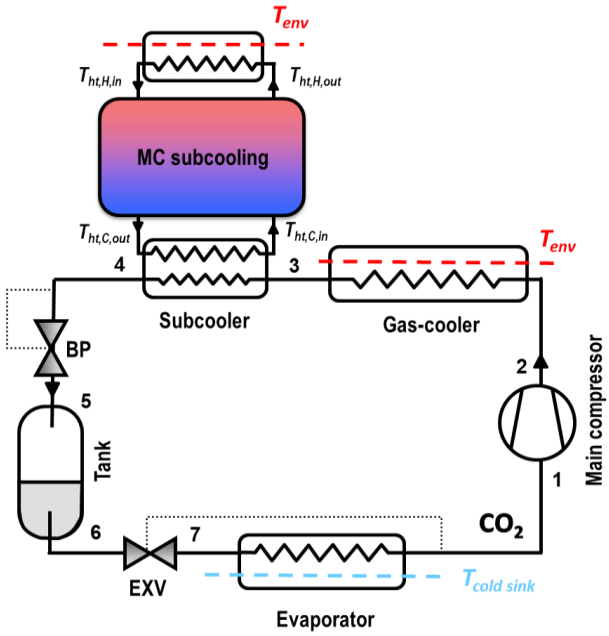

Figure 1. CO_2 transcritical refrigeration plant with magnetocaloric subcooling.

2.1. Transcritical CO_2 refrigeration cycle

The CO_2 cycle is evaluated by fixing the evaporation temperature and considering different environmental temperatures (hot sink). To evaluate the performance of the cycle, pressure drop through the heat exchangers and heat losses to the environment are neglected. Pressure at the gas-cooler and the degree of subcooling can be modified to reach the maximum COP.

The temperature at the exit of the gas-cooler is obtained by considering an approach temperature to the environment to be only 2 K (Eq. (1)), which is justified by the high heat transfer rates of CO_2 in transcritical conditions (Kim et al., 2004) and it is also supported by the data obtained from previous experimental studies (Llopis et al., 2016).

$$T_{gc,o} = T_{env} + APP \tag{1}$$

The subcooling degree is the temperature difference between the gas-cooler exit and the subcooler exit temperatures, as presented by Eq. (2). A constant 10 K superheating degree is considered in the evaporator (see Eq. (3)), which is controlled by the EXV. All the thermodynamic properties of the CO_2 are obtained using Refprop 9.1. (Lemmon et al., 2013).

$$SUB = T_{gc,o} - T_{sub,o} \tag{2}$$

$$T_{suc} = T_0 + 10 \tag{3}$$

Compressor is modelled using the curves for the isentropic and volumetric efficiency (Eq. (4) and coefficients from Table 1), based on data provided by the manufacturer. The CO_2 compressor, semihermetic with a displacement of 3.48 $m^3 \cdot h^{-1}$ and nominal power of 4 kW is considered to run always at nominal speed of 1450 rpm.

$$\eta_v = \eta_i = a_0 + a_1 \cdot P_0 + a_2 \cdot P_{gc} + a_3 \cdot \frac{P_{gc}}{P_0} + a_4 \cdot v_{suc} \tag{4}$$

Table 1. Isentropic and volumetric efficiency coefficients.

	η_v	η_i
a_0	1.0473	0.7634
a_1	0.0031	-0.0021
a_2	-0.0030	0.0013
a_3	0.0012	-0.0571
a_4	-11.1282	0.5425

2.2. Magnetic refrigeration subcooling cycle (MRS)

The simulation of the magnetic refrigeration subcooling (MRS) cycle was carried out by considering performance data obtained during the experimental characterization of a magnetic refrigerator prototype, named 8MAG (Aprea et al., 2014). The considered device is a rotary permanent magnet magnetic refrigerator where the MCM is stationary, and the magnet is rotating. It is characterized by an octagonal shape of the magnetic system and a total number of 8 packed-bed AMRs, supported by an aluminium structure (or magnetocaloric wheel) with 45° spacing. Figure 2 shows a schematic view of the MR prototype.

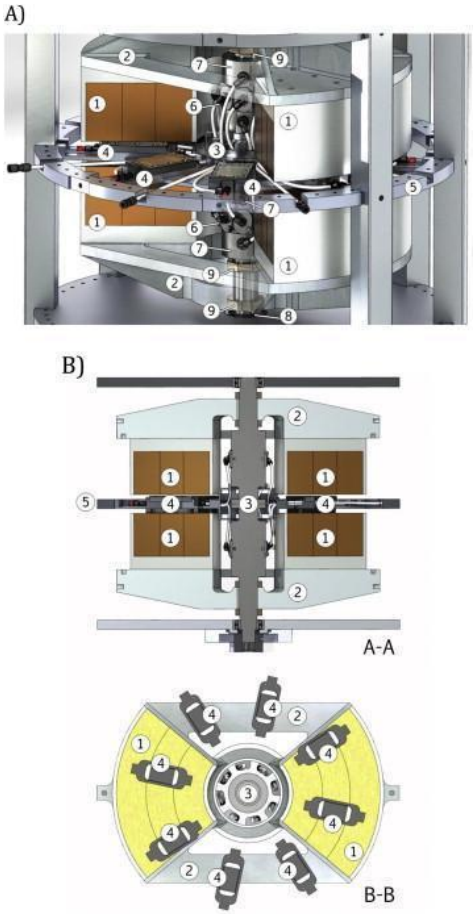

Figure 2. A. MR prototype core details: 1) Permanent magnet assembly. 2) Mounting support. 3) Shaft-rotary valve combination. 4) AMR. 5) Magnetocaloric wheel. 6) Fluid manifold to/from regenerators. 7) Fluid manifold to/from heat exchanger. 8) Bearings. 9) Adjustable rings. B. Longitudinal (A–A) and axial section (B–B) of the device core. (Aprea et al., 2014).

Each AMR has a height of 20 mm, a length of 45 mm, and a width of 35 mm, with 31.5 cm^3 of available volume for the MCM. AMRs were filled with a total mass of 1.2 kg of Gadolinium spheres (400-500 microns) with a purity of 99.82%., which means that each AMR had 150 g of Gadolinium with an average porosity of 0.35. The driving system, consisting of a brushless DC gear-motor rotating the magnets, allows operating with a variable speed in the frequency range between 0.1 Hz and 1 Hz and for every full rotation of the magnetic system, each pair of regenerators undergoes two AMR cycles. Therefore, the MR frequency (f_{MR}) is twice the frequency of the magnetic system (f_{mag}). The MR was tested at different operating conditions in terms of mass flow rate of the heat transfer fluid ($\dot{m}_{ht,MR}$), rotational frequency of the magnets (f_{mag}), temperature of the environment (T_{env}) and temperature span (ΔT_{span}) to characterize its performance, i.e. cooling capacity and COP. The temperature span is defined and calculated as the difference between the heat transfer fluid exiting the hot side of the AMR ($T_{ht,H,o}$) and the heat transfer fluid exiting the cold side of the AMR ($T_{ht,C,o}$), according to Eq. 5.

$$\Delta T_{span} = T_{ht,H,o} - T_{ht,C,o} \tag{5}$$

In Figure 3 the experimental cooling capacity and COP of the MR prototype are shown.

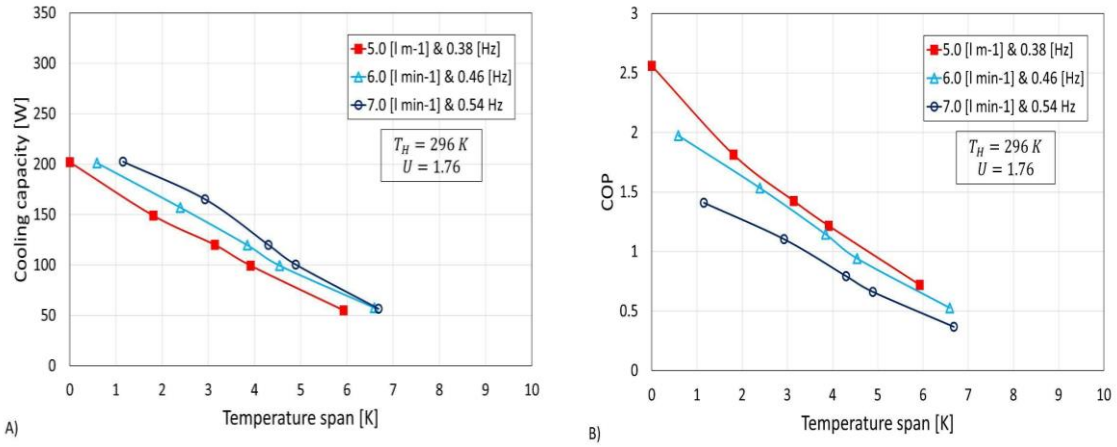

Figure 3. Experimental results of the MR prototype: a) cooling capacity and b) COP (Aprea et al. (2016)).

To integrate the experimental data of the MR prototype into the coupled model of the CO_2 system with a MRS, an Artificial Neural Network (ANN) was developed according to the modelling technique used by Aprea et al. (2017). The scheme of the ANN-based model is depicted in Figure 4. It is characterized by a multi-layer ANN with four input nodes, one hidden layer and two output nodes. The model provides the COP of the magnetic refrigerator (COP_{MR}), as well as the cooling capacity ($\dot{Q}_{MR}$), depending on the temperature span (ΔT_{span}), the rotational frequency of the magnets (f_{mag}), the mass flow of the heat transfer fluid ($\dot{m}_{ht,MR}$) and the temperature of the environment (T_{env}). It should be noted that due to some experimental limitations, the minimum mass flow rate of the heat transfer fluid was 0.08 kg·s^{-1}. However, the results were extrapolated by using the ANN model also to lower mass flow rates assuming the same trends observed experimentally in the range of mass flow rates between 0.08 kg·s^{-1} and 0.12 kg·s^{-1}.

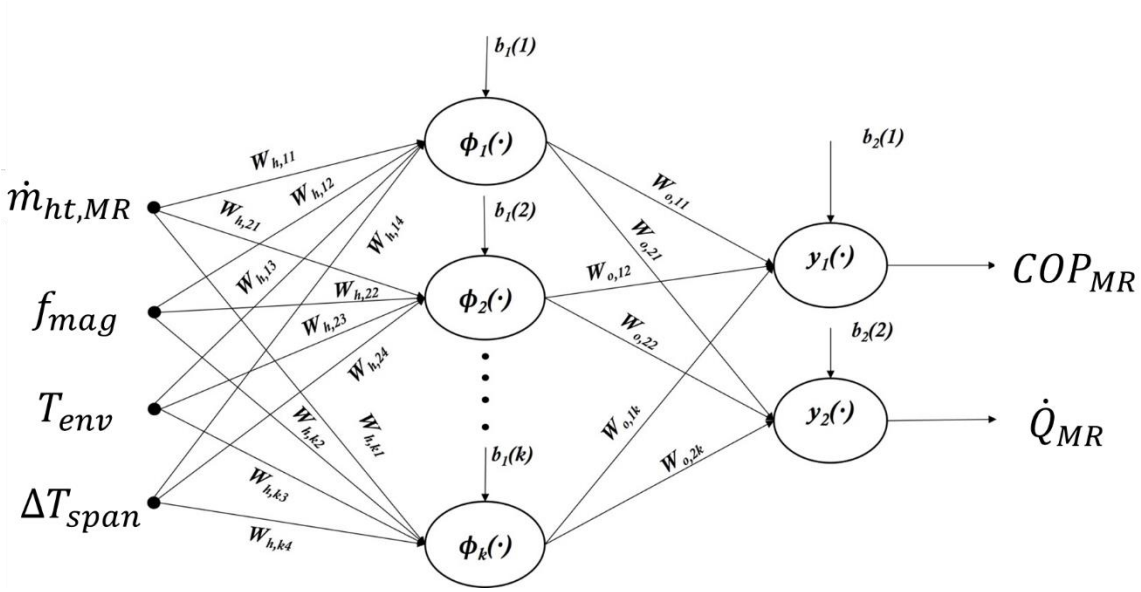

Figure 4. Scheme of the ANN model for the MR system.

The outputs of the ANN model are mathematically represented by Eq.(6-8), as follows:

$$\begin{aligned} &COP_{MR}\left(\dot{m}_{ht,MR}, f_{mag}, T_{env}, \Delta T_{span}\right) \\ &\quad = COP_{MR,min} + \frac{COP_{MR,max} - COP_{MR,min}}{2} \cdot (1 \\ &\quad + \sum_{k=1}^{N_h} \left(w_{1k} \cdot tanh\ tanh\ \left(v_h\left(\dot{m}_{ht,MR}, f_{mag}, T_{env}, \Delta T_{span}\right)\right)\right) \\ &\quad + b_{j=1}) \end{aligned} \tag{6}$$

$$\begin{aligned} &\dot{Q}_{MR}\left(\dot{m}_{ht,MR}, f_{mag}, T_{env}, \Delta T_{span}\right) \\ &\quad = \dot{Q}_{MR,min} + \frac{\dot{Q}_{MR,max} - \dot{Q}_{MR,min}}{2} \cdot (1 \\ &\quad + \sum_{k=1}^{N_h} \left(w_{2k} \cdot tanh\ tanh\ \left(v_h\left(\dot{m}_{ht,MR}, f_{mag}, T_{env}, \Delta T_{span}\right)\right)\right) \\ &\quad + b_{j=2}) \end{aligned} \tag{7}$$

where:

$$\begin{aligned} &v_h\left(\dot{m}_{ht,MR}, f_{mag}, T_{env}, T_{span}\right) \\ &\quad = w_{k1} \cdot \frac{\dot{m}_{ht,MR,min} + \dot{m}_{ht,MR,max} - 2\dot{m}_{ht,MR}}{\dot{m}_{ht,MR,min} - \dot{m}_{ht,MR,max}} + w_{k2} \\ &\quad \cdot \frac{f_{mag,min} + f_{mag,max} - 2f_{mag}}{f_{mag,min} - f_{mag,max}} + w_{k3} \\ &\quad \cdot \frac{T_{env,min} + T_{env,max} - 2T_{env}}{T_{env,min} - T_{env,max}} + w_{k4} \\ &\quad \cdot \frac{\Delta T_{span,min} + \Delta T_{span,max} - 2\Delta T_{span}}{\Delta T_{span,min} - \Delta T_{span,max}} + b_k \end{aligned} \tag{8}$$

In the Eq. (6-8), w_{1k} and w_{2k} represent the parameters of the ANN (synaptic weights) connecting the k-th hidden neurons to the first and second output, i.e. COP and cooling capacity, respectively. On the other

hand, w_{k1}, w_{k2}, w_{k3} and w_{k4} represent the synaptic weights connecting each input node to the k-th hidden neuron. The terms b_k, $b_{j=1}$ and $b_{j=2}$ are the biases of the hidden and output neurons, respectively. The subscripts min and max are referring to the minimum and maximum value of each input and output collected during the experimental tests and they were used to normalize inputs and outputs before the training phase of the ANN (Jayalakshmi and Santhakumaran, 2011).

The learning phase was performed in MatLab environment by using the Levenberg-Marquadt algorithm (Suratgar et al., 2007). The size of the hidden layer N_h can be chosen following trial-and-error procedures (Mohanraj et al., 2012; Sheela and Deepa, 2013) or some empirical rules (Hunter et al., 2012), but an iterative trial-and-error routine was implemented in this case, using the determination coefficient (R^2) to identify the optimal structure of the ANN, calculated as follows:

$$R^2 = 1 - \frac{\sum_{j=1}^{N_o}\sum_{m=1}^{p}\left(Y_{j,m} - y_{j,m}\right)^2}{\sum_{j=1}^{N_o}\sum_{m=1}^{p}\left(Y_{j,m}\right)^2} \tag{9}$$

where $Y_{j,m}$ is the target value of the j-th output for the m-th example, $y_{j,m}$ is the output value predicted by the ANN of the j-th output for the m-th example, N_o is the number of output nodes and p is the number of experimental data pattern. The training routine was performed changing the number of hidden neurons between 9 and 50, leading to an optimal ANN structure characterized by 27 hidden neurons, which provided an R^2 equal to 0.9960, with an average deviation of 4.8 W and 0.04 for the cooling capacity and COP, respectively. To show the results of the training process, the values of the synaptic weights before and after the training are shown in Appendix A.1, as well as an excerpt of the computer code pertaining Eq. 6-8 (Appendix A.2).

To integrate the ANN model of the MR prototype into the CO_2 model, some additional information about the temperatures of the heat transfer fluid were also required. In detail, the temperature of the heat transfer fluid exiting the hot side of the AMR ($T_{ht,H,o}$), is obtained considering an approach temperature with the environmental temperature, as stated in Eq. (10). In several numerical models of AMR cycles (Aprea and Maiorino, 2010; Nakashima et al., 2022; Nielsen et al., 2009; Trevizoli et al., 2016; Tušek et al., 2011), the external heat exchangers were considered as ideal, i.e., with an approach temperature equal to 0. However, in this semi-empirical approach, it was fixed to be equal to 2 K since the maximum approach temperature measured during the experimental tests was equal to 1.8 K (Aprea et al. (2016)).

$$T_{ht,H,o} = T_{env} + APP \tag{10}$$

To ensure the heat transfer in the subcooler and being able to subcool the CO_2, the heat transfer fluid entering the subcooler must always be at a lower temperature than the desired one in the CO_2 subcooler exit. Thus, the $T_{ht,C,o}$ is defined as:

$$T_{ht,C,o} = T_{sub,o} - \Delta T \tag{11}$$

The ΔT in Eq. (11) is considered to be equal to 2 K.

In the end, for the simulation of the MR prototype, some boundary conditions for the input parameters were considered based on the experimental results (Aprea et al., 2016). They are presented in Table 2. In detail, the mass flow rate of the heat transfer fluid and the rotational frequency of the magnets, which represent the operative parameters of the MR device, are varied by steps of 0.005 kg·s^{-1} and 0.1 Hz, respectively.

Table 2. Boundary values of the input parameters of the ANN model for the MR system.

Input parameter	Boundary values

$\dot{m}_{ht,MR}\ (kg \cdot s^{-1})$	0.02-0.12
$f_{mag}\ (Hz)$	0.2-0.8
$T_{env}\ (ºC)$	16-35
$\Delta T_{span}\ (K)$	0-11

2.3. Overall system

Both systems are thermally coupled through the subcooler (Figure 1) and the scheme of the overall model is shown in Figure 5. In detail, it is composed of two sub-models, namely the CO_2 and the MR sub-models as described in the previous Sections. The simulation procedure is as follows. Environmental and evaporation temperatures are the input values of the overall model. The gas-cooler pressure is the input value of the CO_2 model, and it follows an iteration procedure to find the optimal pressure for which the COP is maximum. The value of subcooling degree is also initialized to start the evaluation of the MR system performance. From an initial subcooling degree ($SUB_{attempt}$), the temperature span is calculated and the ANN model simulating the behaviour of the MR prototype is run to find its maximum performance ($COP_{MR,max}$), corresponding to a certain value of mass flow rate of the heat transfer fluid and rotational frequency of the magnets ($\dot{m}_{ht,MR,opt}$ and $f_{mag,opt}$, respectively). As a result, the cooling capacity provided by the MR to the subcooler ($\dot{Q}_{MR} = \dot{Q}_{sub}$) is also obtained. Then, from this data, a new subcooling degree value, which can be achieved with the provided cooling capacity, is recalculated, leading to a new value of the temperature span. This process is iteratively computed until the difference between the new subcooling degree and the previous one is less than a pre-defined value ($\varepsilon = 0.01$) or the maximum number of iterations (equal to 30) is achieved. The latter means that no solution can be found, and the corresponding operating point is not feasible. The iterative process based on the bisection method is marked with red arrows. When the iteration is finished, the overall COP of the coupled system is obtained.

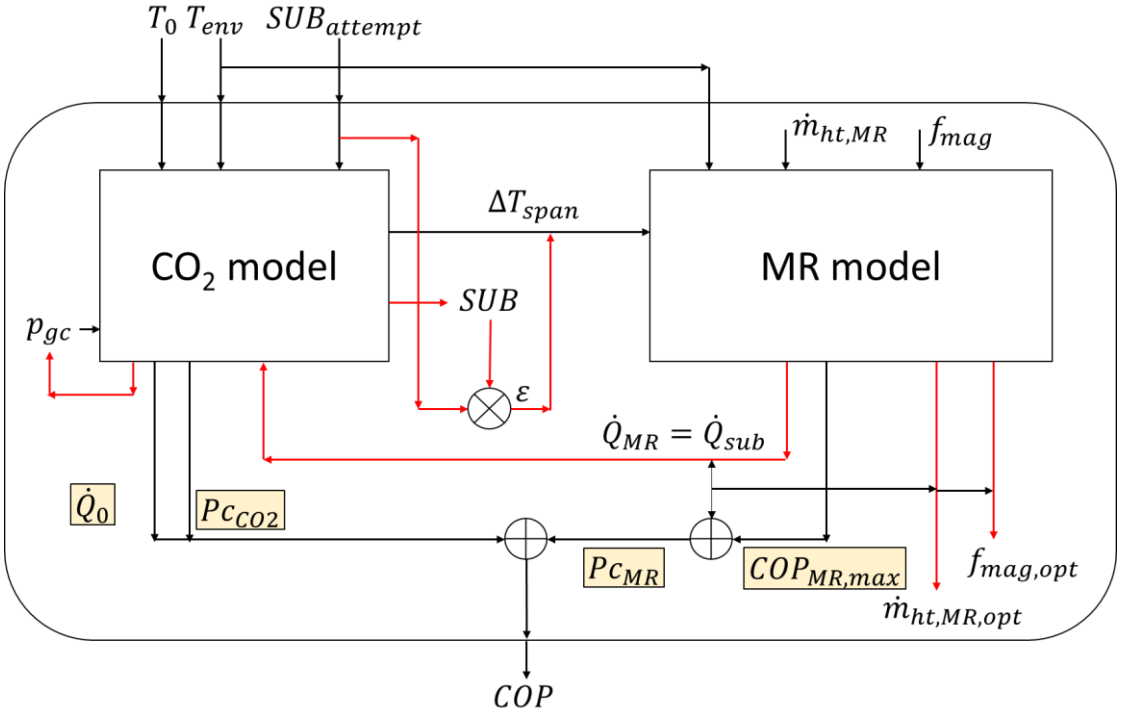

Figure 5. Scheme of the overall computational model.

The complete flow-chart of the coupled model is shown in Figure 6, where the detailed explanation of the computational steps is provided.

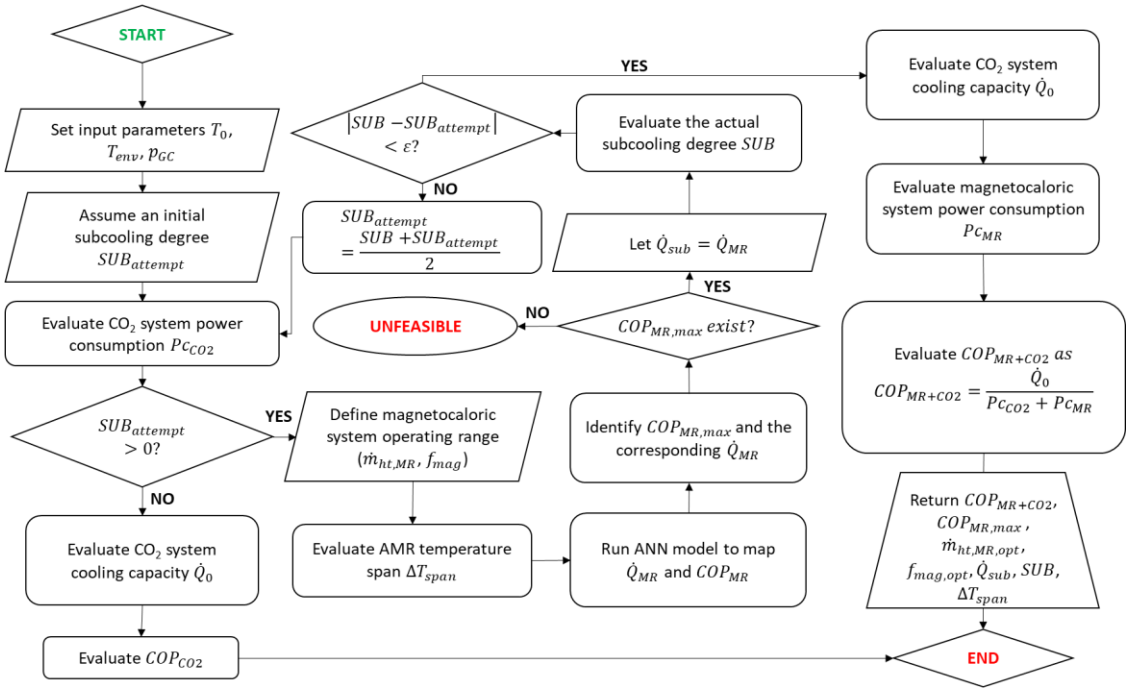

Figure 6. Flow-chart of the coupled model

Power consumption of the CO_2 cycle is evaluated based on the isentropic efficiency, the difference between discharge isentropic enthalpy and suction enthalpy and the mass flow rate, as shown in Eq. (12).

$$Pc_{CO_2} = \dot{m}_{CO_2} \frac{h_{dis,s} - h_{suc}}{\eta_i} \tag{12}$$

Power consumption of the MRS cycle is obtained from the relation between the COP of the MR system and the cooling capacity needed in the subcooler. Cooling capacity in the subcooler is evaluated by Eq. (13). The COP_{MR} is referring to the overall electrical power absorbed by 8MAG, from the electrical motor and the pump.

$$\dot{Q}_{sub} = \dot{m}_{CO_2} \cdot (h_{gc,o} - h_{sub,o}) \tag{13}$$

Then, power consumption of the MRS system is evaluated using Eq. (14). COP_{MR} is evaluated by the ANN model trained on the experimental data, as shown in Eq. (6). The experimental COP was calculated considering the cooling capacity provided by the system and the power absorbed by the pump, used to move the heat transfer fluid, and the electric motor used to move the magnets.

$$Pc_{AMR} = \frac{\dot{Q}_{sub}}{COP_{MR}} \tag{14}$$

The overall COP of the system of CO_2 with MRS is evaluated as expressed by Eq. (15).

$$COP = \frac{\dot{Q}_0}{Pc_{CO_2}+Pc_{MR}} = \frac{\dot{m}_{CO_2}\cdot(h_{suc}-h_{sub,o})}{Pc_{CO_2}+Pc_{MR}} \quad (15)$$

3. Results and discussion

This section explains the optimum operating conditions of the hybrid system and summarizes the main energy performances of the transcritical CO_2 cycle coupled with a MRS system.

3.1. Optimum operating conditions

The aim of this section is to demonstrate the existence of a maximum COP that can be obtained by identifying the optimum gas-cooler pressure and optimum subcooling degree, which corresponds to the value that maximizes the performance of the MRS. First, the impact of the gas-cooler pressure on the performance of the coupled system is analysed. Then, the operating parameters of the MRS system, which are mass flow rate of the heat transfer fluid and rotating frequency of the magnets, are investigated with the aim to optimize its performance.

Figure 7 shows the overall COP as a function gas-cooler pressure obtained at the operating conditions corresponding to the maximum COP of the MR system, at an evaporating level of -15 ºC and environmental temperatures ranging from 25 to 35 ºC. The COP is calculated for the CO_2 cycle without subcooling (black) and for the hybrid system at maximum MR performance (blue). The points with maximum COP are marked with the squared points. As it can be observed, there is an optimum gas-cooler pressure for each condition. Considering the environmental temperature of 25 ºC, it can be seen that the optimum gas-cooler pressure corresponds to the critical pressure. Then, when the environmental temperature increases, the optimum pressure also increases. When comparing to the system without subcooling, reduction in the optimal pressures can be observed, since the COP at the maximal point is higher and it is achieved at a lower pressure. For example, the optimal pressure for the base system at 35 ºC is 91.2 bar while if the subcooling is performed (in blue), the optimal pressure is 88.8 bar. This is one of the benefits of the subcooling of the CO_2, working pressures can be reduced.

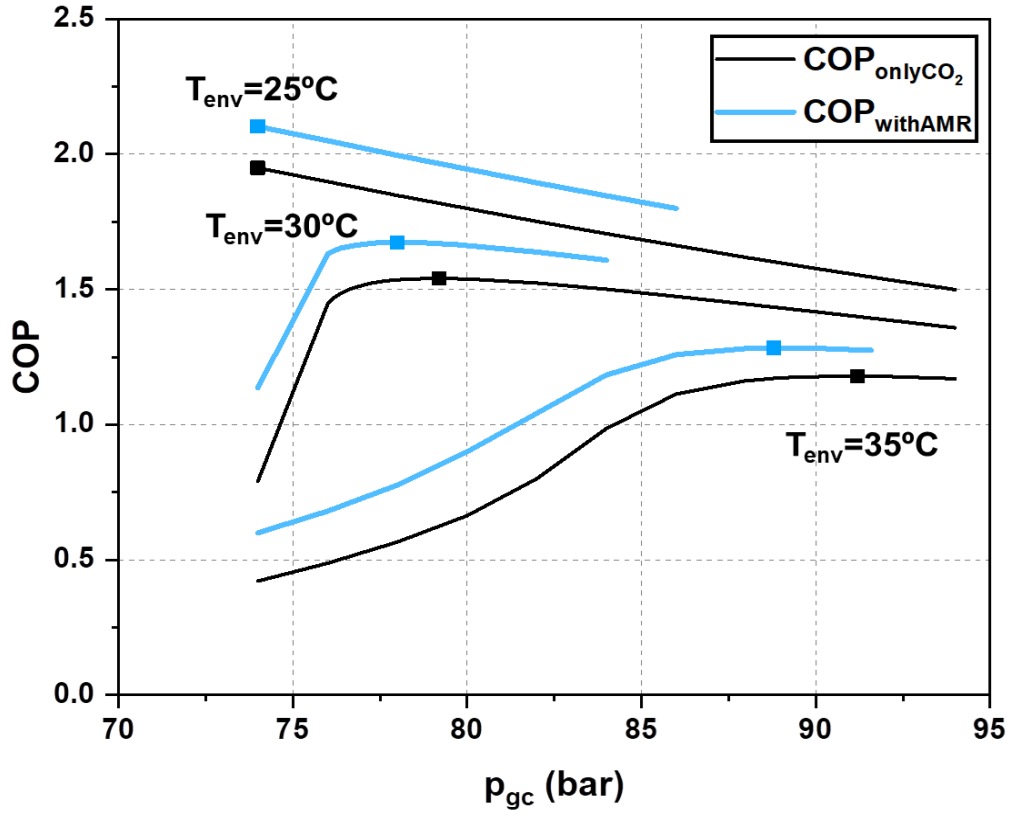

Figure 7. Overall COP evolution as a function of the gas-cooler pressure for different environmental temperatures and evaporation temperature of -15ºC.

The COP of the MR system depends on the mass flow rate of the heat transfer fluid and the MR frequency, which depends on the rotational frequency of the magnets in this case. According to the experimental data (Table 2), values of mass flow rate were changed between 0.02 to 0.12 $kg \cdot s^{-1}$, whereas values of rotational frequency of the magnets were varied between 0.2 and 0.8 Hz, with the aim to identify the optimal combination of operating parameters to maximize the performance of the MRS in terms of the COP for different operating conditions. In detail, simulations were performed for different environmental temperatures from 25 to 35 ºC, and for each of them, the optimal operating point was identified.

As an example, Figure 8 shows the behaviour of the COP (Fig. 8a) and the cooling capacity (Fig. 8b) of the MRS depending on the mass flow rate of the heat transfer fluid and the rotational frequency of the magnets for an evaporating temperature of -15 ºC, with an environmental temperature of 25 ºC and a gas-cooler pressure of 74 bar. The temperature span and environmental temperature are the input values of the MRS model, which affect the possible combinations of mass flow rate of the heat transfer fluid and rotational frequency of the magnets. Therefore, for each environmental temperature, the temperature span is the only parameter which defines the possible coupling of operating parameters values. Among all these possible operating points, the one that provides the maximum COP of the MRS ($COP_{MR,max}$) is selected. The cooling capacity supplied with the corresponding operating conditions is used to recalculate the new subcooling degree provided to the CO_2 system. Considering the example shown in Figure 7, the maximum COP is 3.6 with a cooling capacity of 118 W and a provided subcooling degree of 9 K. This optimal condition of the MRS, marked with the cross symbol, is achieved with a mass flow rate equal to 0.02 $kg \cdot s^{-1}$ and a rotating frequency of the magnets of 0.8 Hz, corresponding to a frequency of the AMR cycle equal to 1.6 Hz.

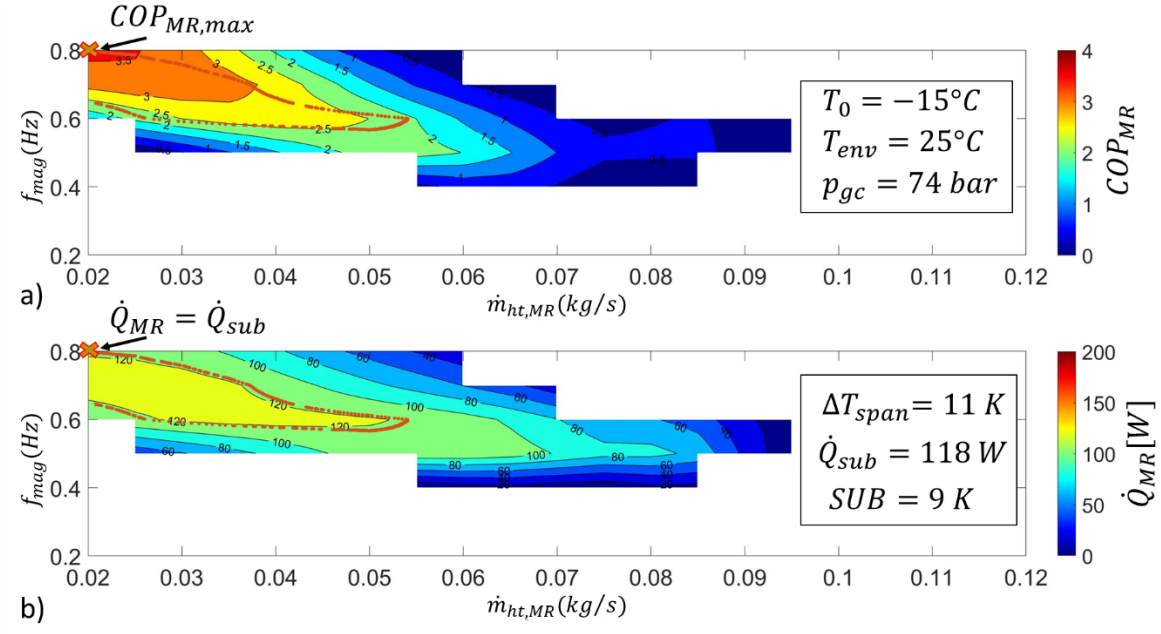

Figure 8. 2-D map of the performance of the magnetic refrigerator depending on the mass flow rate of the heat transfer fluid and rotating frequency of the magnets with $T_{env} = 25\ °C$, $T_0 = -15\ °C$ and $p_{gc} = 74\ bar$: COP_{MR} and b) cooling capacity.

It is worth to highlight that the MRS could work also with different combinations of operating parameters (see the orange line in both Figure 8a-8b). The latter are characterized by different values of temperature span, and consequently of different subcooling degree. However, any other possible combinations lead to decrease in the performance of the magnetic refrigeration system, and therefore they are not considered.

As illustrated in this section, for each condition, there is a value of gas-cooler pressure and COP_{MR} (consequently of subcooling degree) that maximizes the COP of the overall system. Therefore, from now on, all the data presented in the following sections are optimized in terms of gas-cooler pressure and subcooling degree.

3.2. COP and performance improvements

The overall COP for the optimal gas-cooler pressure and optimum COP_{MR} are shown in Figure 9. The COP of the MR corresponding to these optimum points is also presented in this figure. COP of each cycle decreases when the environmental temperature increases. Introducing the subcooling allows to obtain an overall COP higher than the COP of the single CO_2 cycle because the COP of the MR device is higher.

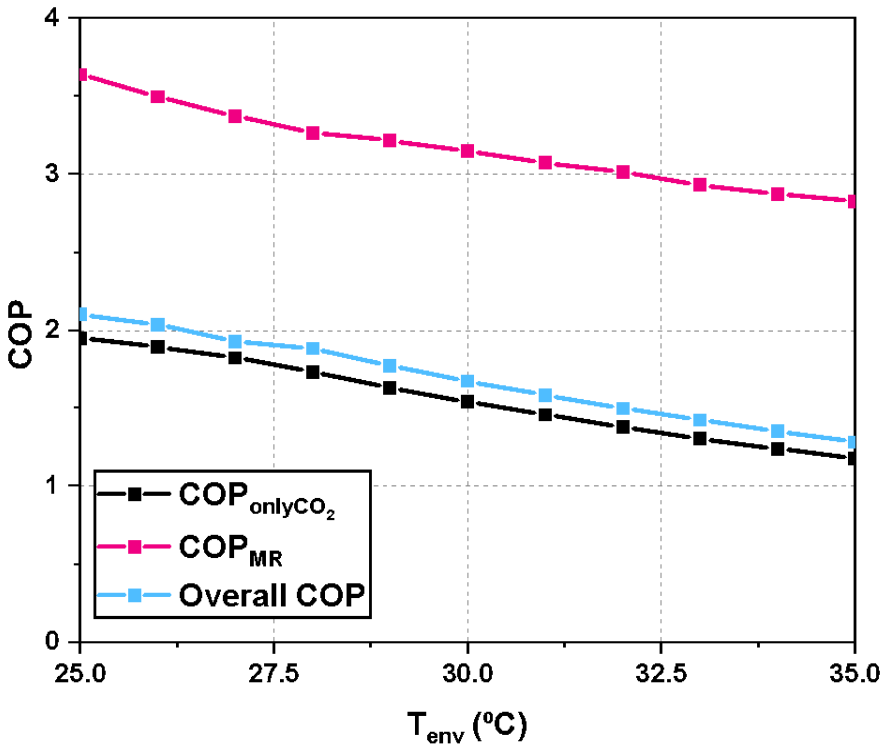

Figure 9. Overall COP and COP of each of the systems individually at optimum conditions.

As it has been said in the introduction, the hybrid of the MR technology with the transcritical CO_2 cycle has the objective of improving the energy performance of the cycle, as it is sought with other subcooling systems. In this work, the optimal operating parameters of the combination of these two technologies have been analysed and the energy performance of the global cycle has been determined. Figure 10 shows the increment in COP achieved by the MRS-CO_2 system with respect to the CO_2 system without subcooling for all the evaluated range. The increments are calculated as shown in Eq. (16).

$$\Delta COP\ (\%) = \frac{COP - COP_{onlyCO_2}}{COP_{onlyCO_2}} \tag{16}$$

As it can be observed, from 25 ºC to 27 ºC there is a reduction in the improvement achieved and then it increases up to values of around 8.8% for the entire temperature range from 28 ºC to 35 ºC with a maximum COP increment of 9.0% obtained at 34 ºC.

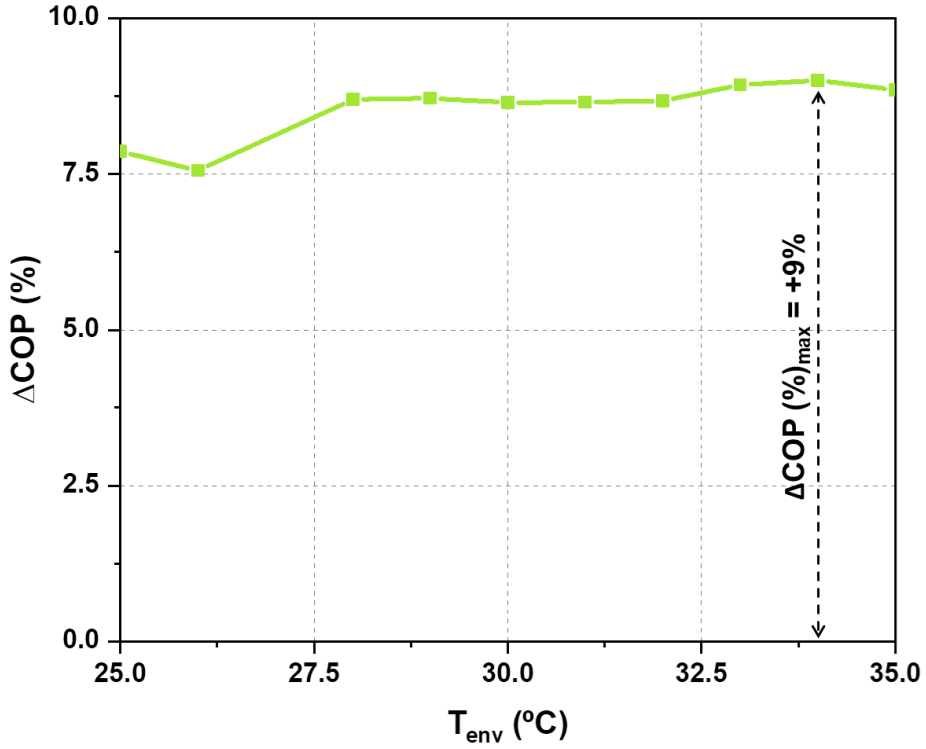

Figure 10. Increments in COP with respect to base system.

Subcooling should provide higher increments at higher ambient temperature (Nebot-Andrés et al., 2022), which is not true in this case. This is because the MR system is designed to work at lower ambient temperatures and its performance at temperatures above 30 ºC is decreasing. This is closely related to the properties of the MCM used in the MR. In the following section, the operation of the MR will be analysed in detail to really understand what happens at these temperatures.

Figure 11 shows the optimum gas-cooler pressure for the MCS-CO_2 system and the system without subcooling depending on the environmental temperature. As it can be seen, optimum gas-cooler pressure increases with the environmental temperature, which is the normal behavior concerning CO_2 systems (Sarkar et al., 2004). The subcooling of CO_2 leads to a reduction of the optimal pressure, as it can be seen in Figure 11. Figure 12 sums up all the pressure reductions achieved by the use of the MRS. Optimal pressure between 25 and 28 ºC is equal to the critical pressure and it is the same for both systems (with and without MR system), so the pressure reduction is equal to 0. It can be seen that when the temperature is higher than 29 ºC, the subcooling allows pressure reductions of up to 2.4 bar.

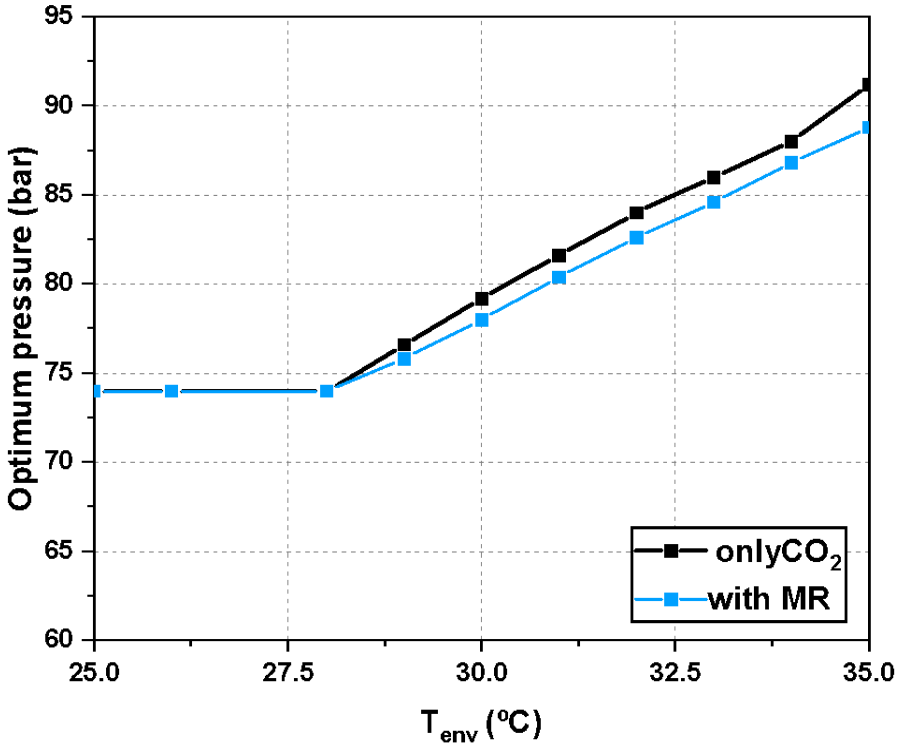

Figure 11. Optimum gas-cooler pressures for the MRS-CO_2 system (blue) and the system without subcooling (black).

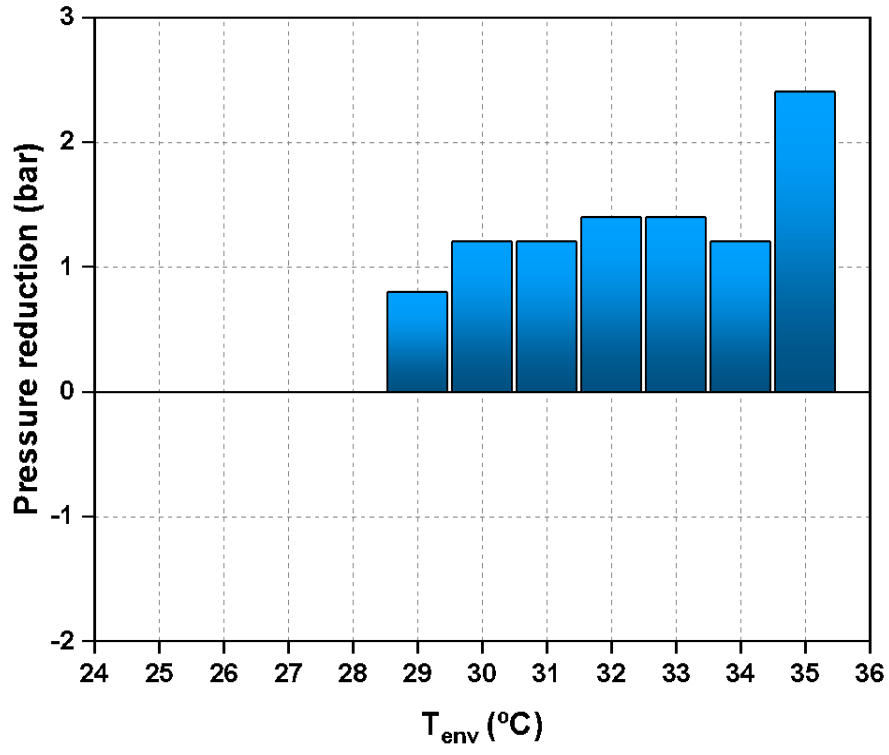

Figure 12. Pressure reduction with respect to the CO_2 system without subcooling.

Figure 13 shows the maximum COP of the MR system and the corresponding temperature span and subcooling degree for different environmental temperature. The MRS is always considered to work with operating parameters which maximise its COP, as shown in Section 3.1. The simulations were performed for different environmental temperatures (between 25 °C and 35 °C), which allowed to analyse the behavior of the optimal operating parameters according to different ambient conditions. In detail, the behavior of mass flow rate of the heat transfer fluid, the rotating frequency of the magnets, and the temperature span, and consequently the subcooling degree, are investigated considering optimal working conditions (i.e. maximum COP of the MRS).

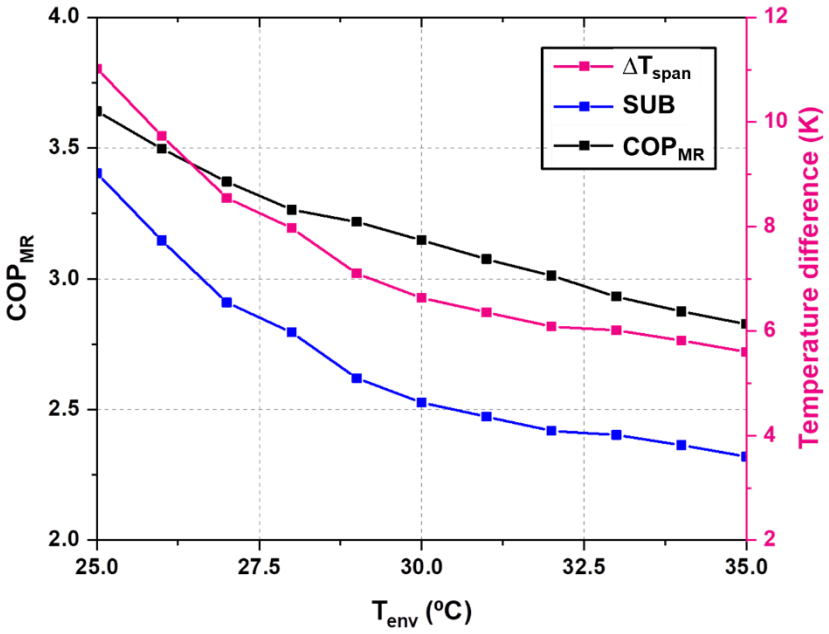

Figure 13. COP of the magnetocaloric system operating in optimal conditions and corresponding temperature span and subcooling degree.

From Figure 13 it is seen how the increase of the environmental temperature leads to decrease the maximum COP of the MRS, and subsequently also the overall COP of the coupled system.

Combining Eq. (10) and Eq. (11) with Eq. (5), the temperature span can be described as a function of the environmental temperature, the subcooler outlet temperature and the approach considered on the subcooler, as described in Eq. (17)

$$\Delta T_{span} = T_{env} + APP - T_{sub,o} + \Delta T \tag{17}$$

Using Eq. (2) and Eq. (1), the Eq. (18) is obtained, where it can be observed that the temperature span only depends on the subcooling degree and the temperature approach considered in subcooler.

$$\Delta T_{span} = SUB + \Delta T \tag{18}$$

As it can be seen from Eq. (18), the temperature span is directly related to the subcooling degree. This is important because higher subcooling degree is favourable for the CO_2 system, but on the other hand, increasing the temperature span results in smaller COP of the MR device. It is therefore necessary to find the compromise between both parameters that maximizes the performance of the overall system.

As the COP of the MRS, the temperature span and subcooling degree decrease as the environmental temperature increases as well. From a point of view, the temperature span behaves accordingly to the data in the literature (Aprea et al., 2014; Lozano et al., 2016), showing a negative slope for environmental

temperatures higher than 25 °C, since the system is working away from the Curie temperature of Gadolinium, which is 20 °C. On the other hand, the behavior of the optimal subcooling degree seems to be different from the classical behavior reported in the literature for CO_2 systems improved with subcooling methods (Nebot-Andrés et al., 2020a; Nebot-Andrés et al., 2021b). Indeed, most of them are characterized by a larger optimal subcooling degree for higher environmental temperatures since the CO_2 without subcooling has lower performance at high hot sink temperatures. Therefore, there is more room for improvements. In detail, the MCM adopted in the MRs can strongly limits the performance of the overall system. Indeed, the MRS should optimally work around the Curie temperature of the MCM (which is the temperature where the magnetocaloric effect achieves the maximum value), but its performance can quickly drop down when the working temperature range is far from the Curie temperature. The maximum performance can be achieved when the systems work as close as possible to the Curie temperature of the material, which is the temperature where the magnetocaloric effect achieves its maximum value since the material undergoes the most significant phase transition.

Therefore, to improve performance at environmental temperatures close to 30 ºC or higher, it would be necessary to design AMRs made of a MCM that has a Curie temperature close to the working point, or to design a multi-layer regenerator which could provide optimal performance for a wider range of working conditions (Maiorino et al., 2021). With this, it would be possible to further increase the COP improvements presented in Figure 10.

Figure 14 shows the optimal values of the rotating frequency of the magnets and mass flow rate of the heat transfer fluid that allows obtaining the maximum COP of the MRS with different environmental temperatures. As it can be seen, almost all the points correspond to the upper limit of the working frequency and the minimum value of the mass flow rate. It means that it is necessary to work very close to the limits of the experimental apparatus to achieve the optimal conditions. Therefore, it is required to design a MRS dedicated to the specified CO_2 system with the aim to further improve the overall performance and to reduce the mechanical stress on the device.

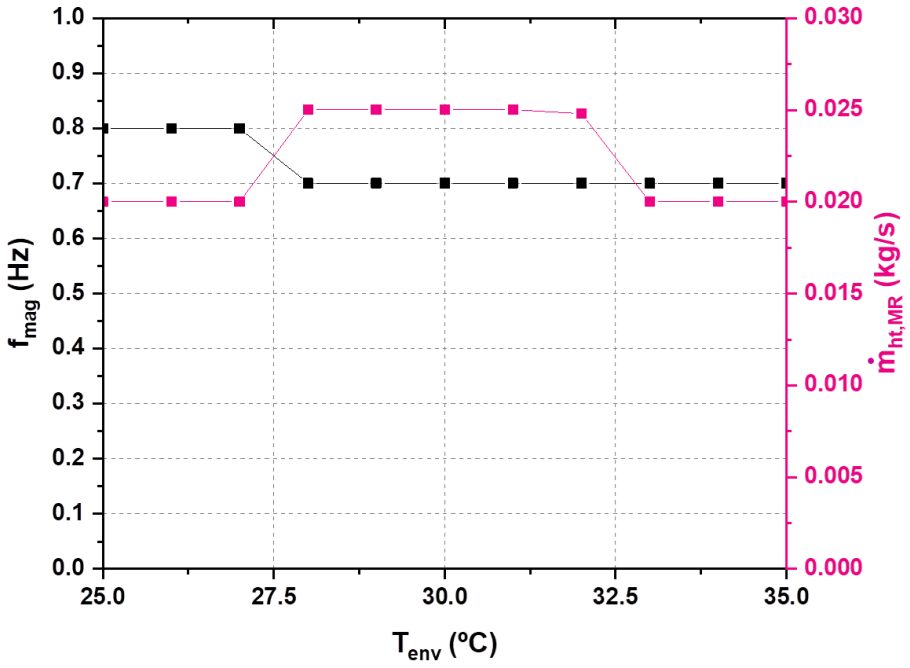

Figure 14. Optimal values of the rotating frequency of the magnets and mass flow rate of the heat transfer fluids to achieve the maximum COP of the MRS with different environmental temperatures.

3.3. Comparison with other methods

Table 3 shows the COP at 25 ºC of environmental temperature and an evaporation temperature of -15 ºC for different CO_2 systems: cycle with parallel compression, cycle with integrated mechanical subcooling (IMS) and with dedicated mechanical subcooling (DMS). All the presented values are optimized and obtained from experimental studies. The COP of the MRS cycle obtained in this work is also included. As it can be seen, the COP values obtained with the MRS system are higher than with the other systems, even if the basis of comparison is not the same, because the parallel compression, the DMS and the IMS are tested experimentally.

Table 3. COP and working conditions of different CO_2 systems at 25 ºC of heat rejection temperature and evaporation temperature of -15 ºC.

Method	Heat rejection temperature (ºC)	T_0 (ºC)	COP	p_{gc} (bar)	SUB (K)	Type	Reference
Parallel compression	24.8	-14.9	1.84	74.4	-	E, O	(Nebot-Andrés et al., 2021a)
Dedicated mechanical subcooling	25.3	-15.5	1.95	74.9	14.3	E, O	(Nebot-Andrés et al., 2021b)
Integrated mechanical subcooling	25.2	-15.6	1.87	74.5	21.3	E, O	(Nebot-Andrés et al., 2020a)
Magnetic refrigeration subcooling	25.0	-15.0	2.10	74.0	9.01	S	This work

E = Experimental, S = Semiempirical, O = Optimized cycle

Performing experimental test of the MRS can lead to lower COP values, but on the other hand designing and optimizing the MR device for this specific application should increase the performance values (Dall'Olio et al., 2021; Masche et al., 2022). The results presented in this work only show the performance that can be achieved with the current state of two existing technologies. This allows establishing a starting point and demonstrating the future potential of this hybridization. Even if these results are not directly comparable with other technologies experimental results, this path can be promising for future investigations and shows that it is a promising technology and that it is worth focusing on its technological development in order to optimize and improve it.

4. Conclusions

This paper presents for the first time a new hybrid system consisting of a CO_2 transcritical refrigeration plant with a magnetic refrigeration system providing subcooling. Magnetic refrigeration is an emerging technology that provides high COPs when working with small temperature span. The temperature differences of the hot sink and cold source of the dedicated subcooling methods are very small, which makes magnetic refrigeration a potential technology for the energy improvement of CO_2 cycles. The evaluation of the fusion of these two technologies has been performed based on previous experimental data.

The study covered in transcritical conditions environmental temperatures from 25 ºC to 35 ºC for the evaporating temperature of -15 ºC. The studied cycle is a transcritical CO_2 single stage refrigeration system with the expansion process performed in two stages with a liquid receiver between both. The magnetic refrigeration system is simulated based on the experimental data obtained from a single-layer packed-bed Gadolinium magnetic refrigerator prototype.

The analysis of the cycle has allowed affirming that there are several variables that must be optimized in this type of systems: the degree of subcooling (related to the temperature span in the magnetic refrigerator), the gas-cooler pressure and the heat transfer fluid mass flow ratio and frequency of the AMR that allow to obtain maximum COP of the magnetic refrigerator. These optimal parameters have been identified and once known, the main energetic parameters of the system have been obtained.

Finally, values of COP are obtained for different ambient conditions reaching values from 2.10 to 1.28 at 25.0 ºC and 35.0 ºC of environmental temperature, respectively. The optimum COP is compared with the COP of the system without subcooling and increments up to 9.0% are obtained for an environmental temperature of 34 ºC with respect to the cycle without subcooling.

Optimum gas-cooler pressure is equal to the critical pressure when the environmental temperature is lower than 28 ºC and, above this temperature it is increasing with temperature, following the same trend as other CO_2 systems. However, this pressure is lower that the optimal pressure for the CO_2 system without subcooling, which is another advantage of the use of this technology.

However, these improvements can be even higher because the magnetic refrigerator prototype was not designed for this purpose. By designing a specific prototype to work in this application and optimizing the magnetic refrigerator by using magnetocaloric materials with optimal Curie temperatures required for subcooling system, a significant increase in efficiency could be obtained. The possibility of recovering expansion work to drive the MR system and improve overall performance can also be explored.

In conclusion, a new subcooling method that produces significant improvements in COP and gives a new application to magnetic refrigeration technology has been presented. Finally, we can affirm that the use of the magnetic refrigeration subcooling cycle as a path to improve the performance of CO_2 transcritical plants needs to be considered and should be studied deeper. Additionally, it needs to be mentioned that these results are semi-empirical and experimental research with the design of a new prototype would be required to quantify exactly the improvements that can be achieved. What is important to conclude is that the technology proposed in this work allows opening a new door to research and, with more future developments, very competitive results can be reached.

Acknowledgements

The authors thank the Ministerio de Educación, Cultura y Deportes - Spain (grant FPU16/00151) and the Ministerio de Universidades – Spain (grant EST21/00293) for financing this research work.

References

Aprea, C., Greco, A., Maiorino, A., 2015. The application of a desiccant wheel to increase the energetic performances of a transcritical cycle. Energy Conversion and Management 89, 222-230.

Aprea, C., Greco, A., Maiorino, A., 2017. An application of the artificial neural network to optimise the energy performances of a magnetic refrigerator. International Journal of Refrigeration 82, 238-251.

Aprea, C., Greco, A., Maiorino, A., Masselli, C., 2016. The energy performances of a rotary permanent magnet magnetic refrigerator. International Journal of Refrigeration 61, 1-11.

Aprea, C., Greco, A., Maiorino, A., Mastrullo, R., Tura, A., 2014. Initial experimental results from a rotary permanent magnet magnetic refrigerator. International Journal of Refrigeration 43, 111-122.

Aprea, C., Maiorino, A., 2010. A flexible numerical model to study an active magnetic refrigerator for near room temperature applications. Applied Energy 87, 2690-2698.

Arora, A., Singh, N.K., Monga, S., Kumar, O., 2011. Energy and exergy analysis of a combined transcritical CO2 compression refrigeration and single effect H2O-LiBr vapour absorption system. International Journal of Exergy 9, 453-471.

Astrain, D., Merino, A., Catalán, L., Aranguren, P., Araiz, M., Sánchez, D., Cabello, R., Llopis, R., 2019. Improvements in the cooling capacity and the COP of a transcritical CO2 refrigeration plant operating with a thermoelectric subcooling system. Applied Thermal Engineering 155, 110-122.

Barclay, J.A., 1982. Use of a ferrofluid as the heat-exchange fluid in a magnetic refrigerator. Journal of Applied Physics 53, 2887-2894.

Beshr, M., Bush, J., Aute, V., Radermacher, R., 2016. Steady state testing and modeling of a CO2 two-stage refrigeration system with mechanical subcooler, Refrigeration Science and Technology, pp. 893-900.

Bush, J., Beshr, M., Aute, V., Radermacher, R., 2017. Experimental evaluation of transcritical CO2 refrigeration with mechanical subcooling. Science and Technology for the Built Environment 23, 1013-1025.

Dall'Olio, S., Masche, M., Liang, J., Insinga, A.R., Eriksen, D., Bjørk, R., Nielsen, K.K., Barcza, A., Vieyra, H.A., Beek, N.V., Bez, H.N., Engelbrecht, K., Bahl, C.R.H., 2021. Novel design of a high efficiency multi-bed active magnetic regenerator heat pump. International Journal of Refrigeration 132, 243-254.

Eriksen, D., Engelbrecht, K., Bahl, C.R.H., Bjørk, R., Nielsen, K.K., Insinga, A.R., Pryds, N., 2015. Design and experimental tests of a rotary active magnetic regenerator prototype. International Journal of Refrigeration 58, 14-21.

European Commission, 2014. Regulation (EU) No 517/2014 of the European Parliament and of the Council of 16 April 2014 on fluorinated greenhouse gases and repealing Regulation (EC) No 842/2006.

Greco, A., Aprea, C., Maiorino, A., Masselli, C., 2019. A review of the state of the art of solid-state caloric cooling processes at room-temperature before 2019. International Journal of Refrigeration 106, 66-88.

Hafner A., Hemmingsen A. K. T., Ven A. van de, 2014. R744 refrigeration system configurations for supermarkets in warm climates, 3rd IIR International Conference on Sustainability and the Cold Chain. Proceedings. International Institute of Refrigeration, London, UK.

Hunter, D., Yu, H., Pukish Iii, M.S., Kolbusz, J., Wilamowski, B.M., 2012. Selection of proper neural network sizes and architectures-A comparative study. IEEE Transactions on Industrial Informatics 8, 228-240.

Jayalakshmi, T., Santhakumaran, A., 2011. Statistical Normalization and Backpropagation for Classification. International Journal of Computer Theory and Engineering 3, 1793-8201.

Kamran, M.S., Ahmad, H.O., Wang, H.S., 2020. Review on the developments of active magnetic regenerator refrigerators – Evaluated by performance. Renewable and Sustainable Energy Reviews 133.

Karampour, M., Sawalha, S., 2016. Integration of heating and air conditioning into a CO2 trans-critical booster system with parallel compression Part I: Evaluation of key operating parameters using field measurements, Refrigeration Science and Technology, pp. 323-331.

Kim, M.H., Pettersen, J., Bullard, C.W., 2004. Fundamental process and system design issues in CO2 vapor compression systems. Progress in Energy and Combustion Science 30, 119-174.

Lawrence, N., Elbel, S., 2016. Experimental study on control methods for transcritical CO2 two-phase ejector systems at off-design conditions, Refrigeration Science and Technology, pp. 511-518.

Lawrence, N., Elbel, S., 2019. Experimental investigation on control methods and strategies for off-design operation of the transcritical R744 two-phase ejector cycle. International Journal of Refrigeration.

Lemmon, E.W., Huber, M.L., McLinden, M.O., 2013. REFPROP, NIST Standard Reference Database 23, v.9.1. National Institute of Standards, Gaithersburg, MD, U.S.A.

Llopis, R., Cabello, R., Sánchez, D., Torrella, E., 2015. Energy improvements of CO2 transcritical refrigeration cycles using dedicated mechanical subcooling. International Journal of Refrigeration 55, 129-141.

Llopis, R., Nebot-Andrés, L., Cabello, R., Sánchez, D., Catalán-Gil, J., 2016. Experimental evaluation of a CO2 transcritical refrigeration plant with dedicated mechanical subcooling. International Journal of Refrigeration 69, 361-368.

Llopis, R., Nebot-Andrés, L., Sánchez, D., Catalán-Gil, J., Cabello, R., 2018. Subcooling methods for CO2 refrigeration cycles: A review. International Journal of Refrigeration 93, 85-107.

Lozano, J.A., Capovilla, M.S., Trevizoli, P.V., Engelbrecht, K., Bahl, C.R.H., Barbosa, J.R., Jr., 2016. Development of a novel rotary magnetic refrigerator. International Journal of Refrigeration 68, 187-197.

Maiorino, A., Del Duca, M.G., Tomc, U., Tušek, J., Kitanovski, A., Aprea, C., 2021. A numerical modelling of a multi-layer LaFeCoSi Active magnetic regenerator by using Artificial Neural Networks. Applied Thermal Engineering 197.

Masche, M., Liang, J., Dall'Olio, S., Engelbrecht, K., Bahl, C.R.H., 2021. Performance analysis of a high-efficiency multi-bed active magnetic regenerator device. Applied Thermal Engineering 199.

Masche, M., Liang, J., Engelbrecht, K., Bahl, C.R.H., 2022. Performance assessment of a rotary active magnetic regenerator prototype using gadolinium. Applied Thermal Engineering 204.

Mohanraj, M., Jayaraj, S., Muraleedharan, C., 2012. Applications of artificial neural networks for refrigeration, air-conditioning and heat pump systems - A review. Renewable and Sustainable Energy Reviews 16, 1340-1358.

Nakashima, A.T.D., Peixer, G.F., Lozano, J.A., Barbosa, J.R., Jr., 2022. A lumped-element magnetic refrigerator model. Applied Thermal Engineering 204.

Nebot-Andrés, L., Calleja-Anta, D., Sánchez, D., Cabello, R., Llopis, R., 2022. Experimental assessment of dedicated and integrated mechanical subcooling systems vs parallel compression in transcritical CO2 refrigeration plants. Energy Conversion and Management 252, 115051.

Nebot-Andrés, L., Catalán-Gil, J., Sánchez, D., Calleja-Anta, D., Cabello, R., Llopis, R., 2020a. Experimental determination of the optimum working conditions of a transcritical CO2 refrigeration plant with integrated mechanical subcooling. International Journal of Refrigeration 113, 266-275.

Nebot-Andrés, L., Sánchez, D., Calleja-Anta, D., Cabello, R., Llopis, R., 2020b. Experimental determination of the optimum working conditions of a commercial transcritical CO2 refrigeration plant with a R-152a dedicated mechanical subcooling. International Journal of Refrigeration.

Nebot-Andrés, L., Sánchez, D., Calleja-Anta, D., Cabello, R., Llopis, R., 2021a. Experimental determination of the optimum intermediate and gas-cooler pressures of a commercial transcritical CO2 refrigeration plant with parallel compression. Applied Thermal Engineering 189.

Nebot-Andrés, L., Sánchez, D., Calleja-Anta, D., Cabello, R., Llopis, R., 2021b. Experimental determination of the optimum working conditions of a commercial transcritical CO2 refrigeration plant with a R-152a dedicated mechanical subcooling. International Journal of Refrigeration 121, 258-268.

Nielsen, K.K., Bahl, C.R.H., Smith, A., Bjørk, R., Pryds, N., Hattel, J., 2009. Detailed numerical modeling of a linear parallel-plate Active Magnetic Regenerator. International Journal of Refrigeration 32, 1478-1486.

Purohit, N., Sharma, V., Sawalha, S., Fricke, B., Llopis, R., Dasgupta, M.S., 2018. Integrated supermarket refrigeration for very high ambient temperature. Energy 165, 572-590.

Rigola, J., Ablanque, N., Pérez-Segarra, C.D., Oliva, A., 2010. Numerical simulation and experimental validation of internal heat exchanger influence on CO2 trans-critical cycle performance. International Journal of Refrigeration 33, 664-674.

Sánchez, D., Aranguren, P., Casi, A., Llopis, R., Cabello, R., Astrain, D., 2020. Experimental enhancement of a CO2 transcritical refrigerating plant including thermoelectric subcooling. International Journal of Refrigeration 120, 178-187.

Sarkar, J., Agrawal, N., 2010. Performance optimization of transcritical CO2 cycle with parallel compression economization. International Journal of Thermal Sciences 49, 838-843.

Sarkar, J., Bhattacharyya, S., Gopal, M.R., 2004. Optimization of a transcritical CO2 heat pump cycle for simultaneous cooling and heating applications. International Journal of Refrigeration 27, 830-838.

Sheela, K.G., Deepa, S.N., 2013. Review on methods to fix number of hidden neurons in neural networks. Mathematical Problems in Engineering 2013.

Suratgar, A.A., Tavakoli, M.B., Hoseinabadi, A., 2007. Modified Levenberg–Marquardt Method for Neural Networks Training. International Journal of Computer and Information Engineering 1, 1745 - 1747.

Trevizoli, P.V., Nakashima, A.T., Barbosa, J.R., Jr., 2016. Performance evaluation of an active magnetic regenerator for cooling applications – part II: Mathematical modeling and thermal losses. International Journal of Refrigeration 72, 206-217.

Tušek, J., Kitanovski, A., Prebil, I., Poredoš, A., 2011. Dynamic operation of an active magnetic regenerator (AMR): Numerical optimization of a packed-bed AMR. International Journal of Refrigeration 34, 1507-1517.

UNEP/TEAP, 1999. The implications to the Montreal Protocol of the inclusion of HFCs and PFCs in the Kyoto Protocol, United States.

Appendix

A.1. Change in the synaptic weights after the training process

Table A.1 Values of the synaptic weights associated with the synapses connecting the inputs and hidden neurons before the training process

	$\dot{m}_{ht,MR}$	f_{mag}	t_{env}	ΔT_{span}	b
N_{h1}	-0.94339	-1.28974	3.093512	-0.73143	3.724436
N_{h2}	-2.25921	-0.88536	1.305825	1.98148	3.728728
N_{h3}	2.110337	-1.38509	2.122081	-1.49498	-3.49973
N_{h4}	-2.66862	2.502554	-0.85602	-1.51053	3.138845
N_{h5}	2.49411	-1.62092	1.256638	1.209305	-3.41745
N_{h6}	0.802151	-1.92516	-2.54259	1.19148	-2.73693
N_{h7}	-3.50477	0.587505	0.948588	0.722832	2.494405
N_{h8}	2.41485	-0.04833	-2.9224	0.396487	-2.23194
N_{h9}	-0.03053	0.628823	-0.12381	3.451798	2.838863
N_{h10}	1.023528	-2.35545	1.201627	-2.5227	-2.096
N_{h11}	2.027893	-1.19315	2.865414	0.096072	-2.10232
N_{h12}	0.738652	3.090258	1.620318	-0.92976	-2.43767
N_{h13}	-3.16404	-0.99316	1.196257	0.68544	2.350195
N_{h14}	1.571177	0.9847	1.275998	2.674245	-2.10178
N_{h15}	3.180997	-1.29248	0.597859	1.428929	-1.69083
N_{h16}	-1.40471	1.244473	2.669367	-1.24769	1.99745
N_{h17}	-1.89351	1.361074	2.286541	0.876853	1.063878
N_{h18}	-2.16302	1.726045	-1.14477	-1.51649	1.295272
N_{h19}	-1.58251	1.705661	-3.04074	-0.62023	0.682558
N_{h20}	-1.76695	-2.60392	-1.68331	1.013477	0.814549
N_{h21}	0.476023	1.893735	1.085511	2.796804	-1.07793
N_{h22}	1.211608	-2.57687	1.241809	1.823479	-0.08729
N_{h23}	0.321331	-2.00663	-1.98461	-2.18223	-0.52207
N_{h24}	1.460218	0.816902	2.242903	2.09573	-0.49559
N_{h25}	-1.85653	2.723629	1.495791	1.172397	0.292429

N_{h26}	2.575687	-0.91501	2.706861	-0.07508	0.152312
N_{h27}	0.339961	-3.67111	-0.41728	0.949812	-1.28354

1

2 Table A.2 Values of the synaptic weights associated with the synapses connecting the inputs and hidden
3 neurons after the training process

	$\dot{m}_{ht,MR}$	f_{mag}	t_{env}	ΔT_{span}	b
N_{h1}	1.047987	-0.39389	-2.33432	1.483472	-3.65012
N_{h2}	0.535301	0.529454	-0.83574	-2.00213	-2.41984
N_{h3}	-2.17166	-1.20087	-0.16584	1.82792	3.029251
N_{h4}	-1.32379	1.799162	-1.1659	-0.97174	2.066108
N_{h5}	-1.26513	-0.01766	0.864803	-2.50552	2.752963
N_{h6}	0.827974	-3.1634	0.316578	-0.95732	-1.99569
N_{h7}	-1.13837	-2.00935	-1.20627	-0.10869	-1.51453
N_{h8}	-2.80814	-1.77112	0.112152	-0.03931	-0.19889
N_{h9}	-0.58041	3.428734	-0.05467	0.221148	1.450539
N_{h10}	3.312933	-0.25925	-2.03276	-0.47667	-0.09995
N_{h11}	0.586848	1.07881	2.282147	1.628111	0.489131
N_{h12}	-0.51293	-1.40238	-1.08912	-2.21064	-0.39503
N_{h13}	-0.60408	1.392884	-0.74947	-1.69252	-0.48795
N_{h14}	-1.04731	1.258227	-1.48563	-1.99034	-0.65495
N_{h15}	-0.80131	-0.15356	1.068742	-2.17088	-0.76183
N_{h16}	-0.42187	4.398275	0.030929	-1.03656	2.825442
N_{h17}	-0.53025	-1.16838	2.129564	-0.77052	-1.80935
N_{h18}	0.299357	-3.00427	0.019773	0.994305	-2.10648
N_{h19}	1.510134	-1.87113	2.684765	0.059701	0.538973
N_{h20}	0.174994	2.142209	0.274178	0.525565	-0.93244
N_{h21}	-1.36397	0.296641	1.428942	-3.18693	-1.13571
N_{h22}	0.826656	2.728666	-0.20276	-0.52838	3.244822
N_{h23}	1.86905	1.000462	-0.09844	-1.34913	2.702464
N_{h24}	-1.55088	0.404929	0.316511	2.822485	-2.4374

N_{h25}	1.644039	2.541612	-0.04219	-0.30804	3.304448
N_{h26}	-3.60392	-0.14224	-1.90892	-0.1066	-3.21727
N_{h27}	-0.86623	-0.36737	-0.33185	-3.18254	-3.9562

1

2 Table A.3 Values of the synaptic weights associated with the synapses connecting the hidden neurons
3 and the outputs before the training process

	COP_{MR}	$\dot{Q}_{MR}$
N_{h1}	0.543383	0.177871
N_{h2}	-0.1638	0.142339
N_{h3}	-0.37106	-0.36432
N_{h4}	0.57606	0.240787
N_{h5}	0.767952	0.547431
N_{h6}	0.082809	0.160361
N_{h7}	0.05424	0.072979
N_{h8}	0.05097	-0.03919
N_{h9}	-0.29244	-0.26873
N_{h10}	-0.13399	-0.07782
N_{h11}	-0.14925	-0.03439
N_{h12}	-0.06616	-0.04763
N_{h13}	-0.23715	-0.26993
N_{h14}	-0.06278	0.028326
N_{h15}	0.100867	-0.08765
N_{h16}	0.212676	0.28105
N_{h17}	0.175697	0.084387
N_{h18}	-0.13984	-0.18189
N_{h19}	-0.59876	-0.52349
N_{h20}	-0.18878	-0.12269
N_{h21}	-0.17251	-0.15902
N_{h22}	-0.18978	-0.19275
N_{h23}	-0.09427	-0.09198

N_{h24}	-0.07012	0.049085
N_{h25}	-0.24129	-0.19088
N_{h26}	-0.24537	-0.19736
N_{h27}	-0.16594	-0.23573
b	-1.5185	-1.2217

1

2 Table A.4 Values of the synaptic weights associated with the synapses connecting the hidden neurons
3 and the outputs after the training process

	COP_{MR}	$\dot{Q}_{MR}$
N_{h1}	-0.47318	-0.60077
N_{h2}	0.192569	-0.10631
N_{h3}	-0.11322	-0.19806
N_{h4}	-0.02559	-0.22609
N_{h5}	-0.15269	-0.38231
N_{h6}	-0.43459	-0.32155
N_{h7}	0.194892	0.280153
N_{h8}	-0.17975	-0.01721
N_{h9}	-0.78529	-0.74655
N_{h10}	-0.19511	-0.24228
N_{h11}	0.091006	-0.13448
N_{h12}	-0.02618	-0.16726
N_{h13}	0.471035	0.605773
N_{h14}	-0.21237	-0.38835
N_{h15}	-0.14282	-0.38472
N_{h16}	-1.87491	-2.14543
N_{h17}	-0.30491	-0.19888
N_{h18}	-3.24064	-3.52381
N_{h19}	-0.05518	-0.07082
N_{h20}	-0.6865	-0.50486
N_{h21}	0.109005	0.300677

N_{h22}	0.53005	2.264142
N_{h23}	-0.64937	-0.59772
N_{h24}	-0.17163	-0.1306
N_{h25}	0.033121	-1.15469
N_{h26}	-0.35571	-0.53411
N_{h27}	0.210589	0.358907
b	-2.0587	-2.4501

1

2

A.2. Section of the computer code to run the ANN

The code to run the ANN according to Eq.6-8 is divided into three parts characterized by three different functions. The first one is needed to normalize the input variables, as follows:

```
function [i_n]=Test_normalization(ingressi,map_i)
Ni=size(ingressi,1);
pattern=size(ingressi,2);
maxinput=map_i(2,:);
mininput=map_i(1,:);
i_n=zeros(Ni,pattern);
for i=1:1:Ni
        for l=1:1:pattern
        i_n(i,l)=-1+2*(ingressi(i,l)-mininput(i))/(maxinput(i)-mininput(i));
        end
end
```

In the code, the variable *map_i*, taken as an input of the function, contains the maximum and minimum values of each input. This section returns the normalized input values (*i_n*).

The second part is the core of the ANN computation, and it represents the forward pass to propagate the input throughout the neurons. It is shown below.

```
function [output]=tanlin_ANN(in,Wh,Wo)
HL=size(Wh,1);
IL=size(Wh,2)-1;
OL=size(Wo,1);
pattern=size(in,2);
H=zeros(HL,pattern);
output=zeros(OL,pattern);
for p=1:1:pattern
        for k=1:1:HL
        v=0;
        for i=1:1:IL
        v=v+Wh(k,i)*in(i,p);
        end
        v=v+Wh(k,IL+1);
    H(k,p)=2/(1+exp(-2*v))-1;
        end
        for j=1:1:OL
        v=0;
        for k=1:1:HL
        v=v+Wo(j,k)*H(k,p);
        end
        v=v+Wo(j,HL+1);
        output(j,p)=v;
        end
end
```

1

This code allows to evaluate the normalized outputs of the ANN considering the normalized inputs calculated with the previous code and the parameters of the ANN, i.e. the synaptic weights (*Wh* and *Wo*). The latter are shown in Tab. A.2 (*Wh*) and Tab. A.4 (*Wo*).

In the end, since the previous step returns the normalized output values, there is a last section needed to obtain the real values of the outputs, as follows:

```
function [output]=denormalize(output_n,map_t)
pattern=size(output_n,2);
No=size(output_n,1);
output=zeros(No,pattern);
maxtarget=map_t(2,:);
mintarget=map_t(1,:);
for j=1:1:No
   for p=1:1:pattern
      output(j,p)=(output_n(j,p)*(maxtarget(j)-mintarget(j))+mintarget(j)+maxtarget(j))./2;
   end
end
```

In the code, the variable *map_t*, taken as an input of the function, contains the maximum and minimum values of each output.